Astronomy & Astrophysics manuscript no. 15559txt
January 26, 2013

© ESO 2013

arXiv:1105.5579v1 [astro-ph.HE] 27 May 2011

Multi-wavelength environment of the Galactic globular cluster Terzan 5

A.-C. Clapson[1,2], W. Domainko[1], M. Jamrozy[3], M. Dyrda[4] and P. Eger[5]

[1] Max-Planck-Institut für Kernphysik, P.O. Box 103980, D 69029 Heidelberg, Germany
[2] EMBL Heidelberg, Meyerhofstrasse 1, D 69117 Heidelberg, Germany
[3] Obserwatorium Astronomiczne, Uniwersytet Jagielloński, ul. Orla 171, 30-244 Kraków, Poland
[4] Instytut Fizyki Jądrowej PAN, ul. Radzikowskiego 152, 31-342 Kraków, Poland
[5] Universität Erlangen-Nürnberg, Physikalisches Institut, Erwin-Rommel-Str. 1, D 91058 Erlangen, Germany

Received August 10, 2010; accepted May 23, 2011

ABSTRACT

Terzan 5 is a Galactic globular cluster exhibiting prominent X-ray and gamma-ray emission. Following the discovery of extended X-ray emission in this object, we explore here archival data at several wavelengths for other unexpected emission features in the vicinity of this globular cluster. Radio data from the Effelsberg 100 metre telescope show several extended structures near Terzan 5, albeit with large uncertainties in the flux estimates and no reliable radio spectral index. In particular, a radio source extending from the location of Terzan 5 to the north-west could result from long-term non-thermal electron production by the large population of milli-second pulsars in this globular cluster. Another prominent radio structure close to Terzan 5 may be explained by ionised material produced by a field O star. As for the diffuse X-ray emission found in Terzan 5, its extension appears to be limited to within 2.5 arcmin of the globular cluster and the available multi-wavelength data is compatible with an inverse Compton scenario but disfavours a non-thermal Bremsstrahlung origin.

Key words. Galaxy:globular clusters: individual: Terzan 5 — Radiation mechanisms: general — Stars:massive

1. Introduction

Terzan 5 is a Galactic globular cluster (GC) located in the inner Galaxy, at R.A. 17^h 48^m 04.0^s and Dec -24° 46' 45" (in Galactic coordinates: l 3.8°, b 1.69°), at 5.9 kpc from the Sun (Ferraro et al., 2009). Terzan 5 hosts the largest population of millisecond pulsars (msPSRs) detected so far (33, Ransom, 2008), and it exhibits the highest central stellar density among Galactic GCs (Lanzoni et al., 2010).

Recent observational results on Terzan 5 concerning non-thermal signatures have renewed the interest in this object. Eger et al. (2010) report diffuse X-ray emission extending beyond the half-mass radius of the GC ($r_h = 0.52'$, Lanzoni et al., 2010) with a hard spectrum of index close to 1, likely of non-thermal origin. In the high-energy γ-ray range (100 MeV < E_γ < 100 GeV) Terzan 5 is the brightest GC seen with *Fermi*-LAT (Kong et al., 2010; Abdo et al., 2010). The γ-ray spectrum of the source is best fitted by a power law with an exponential cut-off at a few GeV, as expected for a population of msPSRs. Kong et al. (2010) also report tentative evidence of a second component in the γ-ray spectrum at energies above 10 GeV, which they interpret as inverse Compton (IC) up-scattering of cluster stellar photons by high-energy electrons. These observations clearly point to a considerable population of non-thermal particles in Terzan 5.

Several models have been proposed that could explain the observed high-energy emission, based for some on leptons accelerated by the population of msPSRs in the GC (e.g. see Bednarek & Sitarek, 2007; Venter & de Jager, 2008; Venter et al., 2009). These models apply in principle to any GC hosting msPSRs. The largest predicted fluxes (based on the known msPSRs) are from 47 Tucanae, also detected by *Fermi*-LAT (Abdo et al., 2009) and Terzan 5, where Abdo et al. (2010) estimate a population of 180 msPSRs, with a large uncertainty. Since different emission processes may dominate in the GeV range and at much lower energies, there is no reason *a priori* for 47 Tucanae to be brighter than Terzan 5 in all parts of the spectrum. Another contribution to the high-energy emission may come from stellar binaries consisting of a normal star and a compact object, accelerating particles to the required energies possibly via non-thermal radio-emitting plasma ejections (described e.g. in Fender et al., 1999). Due to its high core density favourable to dynamical interactions between stellar objects, Terzan 5 is expected to contain many binary systems (e.g. Pooley & Hut, 2006; Ivanova et al., 2008). This would also favour merger events, including white dwarf mergers (see e.g. Shara & Hurley, 2002) and neutron star mergers (discussed in Grindlay et al., 2006), expected to result in explosive events, type Ia supernovae or short gamma-ray bursts (GRBs) depending on the progenitors (white dwarfs and neutron stars respectively). The remnants of these explosions may then be particle-acceleration sites (see e.g. Koyama et al., 1995; Domainko & Ruffert, 2005, 2008).

A scenario for extended X-ray emission in relation to GCs is proposed in Okada et al. (2007). They suggest that supersonic motion through the interstellar medium (ISM) and bow-shock formation are possible for GCs. They also find potential signatures of particles accelerated in GC bow-shocks in radio and X-ray data. Typical three-dimensional velocities of GC are around 200 km/s, but can be as high as 400 km/s for, e.g., NGC 5904 (Okada et al., 2007). Proper motion is unfortunately not avail-

---

Send offprint requests to: e-mail: `clapson@mpi-hd.mpg.de`

able for Terzan 5. Its radial velocity, a lower limit to the total three-dimensional velocity, is about 80 km/s (Harris, 1996).

Previous radio studies of Galactic GCs (see e.g. Gopal-Krishna & Steppe, 1980) have reported flat-spectrum radio sources, some of which (M 3 and M 92) surrounded by arcmin-scale radio features.

Many studies have focused on the GC Terzan 5 itself, if not on its core. Our aim here, prompted by the discovery of X-ray diffuse emission (Eger et al., 2010), is to collect information from archival data over spatial scales from the arcmin to the degree, with particular interest in indications of non-thermal emission processes. This paper is organised as follows. First, measurements from archival data of the region around Terzan 5 are presented. Radio data are discussed in Section 2, X-ray in Section 3, and infrared in Section 4.1. The density of molecular material is investigated in Section 4.2 and possible counterparts from astronomical catalogues are mentioned in Section 5. Then, in Section 6 the implication of our findings on the underlying physical processes are discussed.

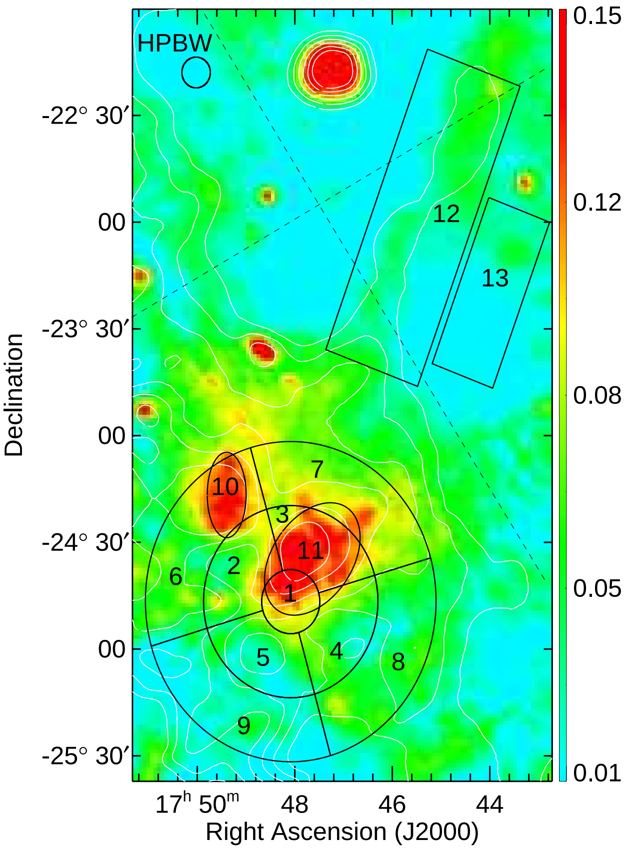

Fig. 1. Radio map from the Effelsberg Galactic plane surveys at 11 cm (in Jy/beam). Contours from the 21 cm map are overplotted (for levels 0.2 to 0.7 Jy/beam per 0.1 step), as well as the regions of Table 1. The region labelled 1 is centred on Terzan 5. The HPBW for the 11 cm data is also shown. The dashed lines indicate the radio scan directions at 11 cm.

2. Radio survey data

Fruchter & Goss (2000) observed Terzan 5 at wavelengths of 90, 20 and 6 cm with high angular-resolutions using the VLA in its three most extended configurations. Their radio maps display numerous point sources with steep spectra, as expected for pulsars. Terzan 5 is also detected in the 21 cm NVSS survey (Condon et al., 1998) as a 5 mJy single source, with a weak polarisation feature extending north of the GC.

2.1. Effelsberg survey data

For the radio analysis of Terzan 5 we used archival 21 and 11 cm (respectively 1408 and 2695 MHz) total intensity maps from the Survey Sampler[1] of the Max Planck Institute for Radio Astronomy. These observations were done with the Effelsberg 100-m telescope as part of Galactic plane surveys. Since we are interested in small-scale structures, we used the 'source-component' maps, which do not contain the global steep-spectrum diffuse Galactic emission. Full details on the data and the processing can be found in Reich et al. (1990a,b). The analysis presented in this paper relies on this preprocessing. The flux density (S) calibration for the dataset was checked by mapping the point-like source 3C286 and adopting the scale of Baars et al. (1977): flux densities of 14.4 (at 21 cm) and 10.4 Jy (at 11 cm). The angular resolution (half-power beam width, HPBW) of the maps are 9′.4 and 4′.3, their sensitivity (noise rms) 40 and 20 mK T_B, and the ratios $T_B[K]/S[Jy]$ are 2.03 ± 0.04 and 2.51 ± 0.05, respectively for 21 and 11 cm (T_B the brightness temperature). The resulting flux maps are shown in Figure 1 and 4.

Region number	R_{min}	R_{max}	ϕ_{min}	ϕ_{max}	Area
		[deg]			$[10^{-6}$ sr]
1	0.0	0.15	0	360	22.59
2	0.15	0.45	-106	-16	45.17
3			-16	74	
4			74	164	
5			164	-106	
6	0.45	0.75	-106	-16	90.34
7			-16	74	
8			74	164	
9			164	-106	
10	0.1	0.2	0	–	19.13
11	0.2	0.3	40	–	57.39
12	0.5	1.5	20	–	228.46
13	0.33	0.83	20	–	84.61

Table 1. Description of the regions defined from the radio maps. Regions 1 is a circle, regions 2 to 9 are circle wedges, all centred on the core position of Terzan 5. Regions 10 and 11 are ellipses, of centres RADec (267.35°, -24.28°) and (266.91°, -24.58°), major and minor axes R_{max} and R_{min} and inclination ϕ_{min}. Region 12 is a rectangular box, centred on RADec (266.35°, -22.98°), of side lengths R_{min} and R_{max} and inclination ϕ_{min}. The rotation angles are relative to north, westwards.

2.2. Regions of interest

The regions used in this work were defined from visual inspection of the Effelsberg radio data. Several features can be seen around Terzan 5, but none exhibits tell-tale morphology (e.g.

---

[1] http://www.mpifr-bonn.mpg.de/survey.html

shell-like or bow-shock-like structure) suggestive of its origin. Ring segments centred on the GC were defined to cover its environment. The width of the rings matches the angular resolution of the radio data, while their orientation aims at isolating main flux levels differences. Two elliptical regions and a rectangular region cover distinct prominent higher flux features, visible in Figure 1. The geometry of all the regions is given in Table 1 and shown in Figure 1.

The radio flux densities of the regions were extracted using the AIPS[2] task IRING, or IMEAN for regions 12 and 13. The error on the radio flux in a region was derived following Klein et al. (2003) :

$$\Delta S_i = \sqrt{(S_i \times \Delta S_c)^2 + (\Delta S_i^n)^2 + (\Delta S_i^z)^2} \qquad (1)$$

for S_i the flux measurement at frequency ν_i and ΔS_i the related error. We used a calibration error ΔS_c of 3% and a noise rms ΔS_i^n derived from the rms noise of the map (respectively 0.08 and 0.05 Jy/beam at 21 and 11 cm) and multiplied the results by the integration area. The estimation of a ‘diffuse-component’ performed by Reich et al. (1990a,b) may locally produce large inaccuracies. The ’diffuse-component’ was subtracted from the original data to obtain the ’source-component’ map used here. We consider a zero-level error ΔS_i^z at 3% of the mean flux value in the region of the ‘diffuse-component’ map. ΔS_i^z also depends on the area (in units of solid angle, used to determine the zero-level). ΔS_i^z is the predominant contribution to the flux errors.

The flux density values are summarised in Table 2. Regions 4, 5 and 8 might indicate local background levels at 11 and 21 cm, with a possible deviation for region 9 (below at 11 cm, above at 21 cm). While two bright regions (10 an 11) stand out at both wavelengths, it is difficult to make out other features, in particular at 21 cm, where the errors are larger and the resolution worse. Regions 1, 2, 3, 6 and 7 overlap somewhat with the bright features and present as expected intermediate flux values.

Region 12 is visible only because of the very low flux densities in its surroundings. Since it is located at higher galactic latitudes the background level of the radio emission is considerably lower than close to Terzan 5. To quantify the robustness of the structure we estimated the background level of the flux density in region 13, adjacent to region 12 at the same galactic latitude (see Table 2). At least at 21 cm, region 12 stands significantly above the local background level.

2.3. Spectral index estimation

We extracted the mean spectral index α for each region from the two flux measurements in each region. The uncertainty on α, estimated following equation 3 of O’Dea et al. (2009) is very large in all regions. We therefore do not present the radio spectral information in this paper. For the discussion we use a spectral index of -0.8. Detailed re-analysis of the archival data or additional data spanning a wider frequency range may reduce this limitation.

3. X-ray data

3.1. ROSAT

The first detection of extended diffuse emission from the GC Terzan 5 was reported by Eger et al. (2010) who analysed the data of an archival *Chandra* Advanced CCD Imaging Spectrometre (ACIS) observation. Following this discovery we investigated archival *ROSAT* data, to search for diffuse emission on a much larger spatial scale than possible with the limited field of view (FoV) of *Chandra*. Terzan 5 was observed by *ROSAT* several times (see e.g. Johnston et al., 1995). We focused on a pointing observation centred on Terzan 5 taken in 1991 (ID 300060) by the High Resolution Imager (HRI) instrument with a total live time of 22.5 ks. The advantage of the *ROSAT*-HRI observation compared to *Chandra* is its large square FoV with a side of 38′. Data analysis relied on the standard packages FTOOLS 5.9 from HEASOFT version 6.8 (Blackburn, 1995) and CIAO[3].

To search for extended diffuse emission, point-like sources must first be excluded. There are 50 Chandra point-sources inside r_h, listed in Table 1 of Heinke et al. (2006). To account for the difference between the point spread function (PSF) of *ROSAT*-HRI (∼ 5″, Boese, 2000) and *Chandra*-ACIS (∼ 1″, Karovska et al., 2001), we defined a large exclusion region at the centre of the GC, with a radius equal to r_h. Outside r_h, Heinke et al. (2006) found 78 *Chandra* sources (listed in their Table 2). We excluded them taking into account the HRI PSF. All the excluded regions were removed from the dataset and refilled with the CIAO DMFILTH tool, assuming Poisson statistics.

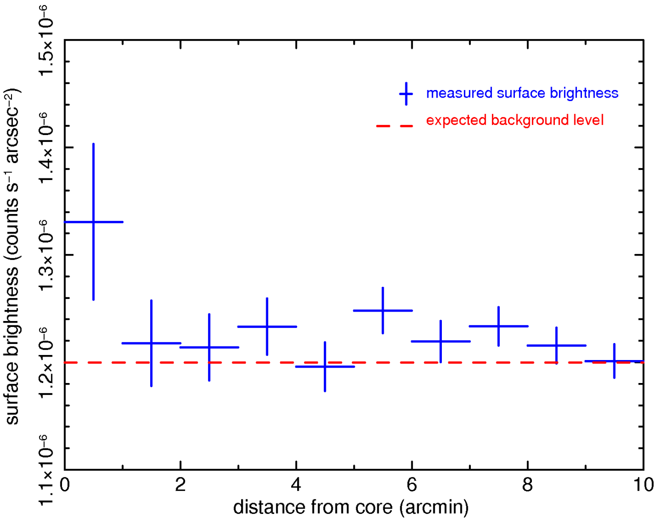

Fig. 2. *ROSAT*-HRI surface brightness versus distance from the core position of Terzan 5, with a 1 σ error bar. The expected background level is represented by the dashed horizontal line. The extraction regions are adjacent rings of equal width, see text for details.

Since the spectral resolution of the HRI camera is very limited, we only extracted the total count-rate in the full HRI energy band (0.1 – 2.4 keV). The HRI background is discussed in the *ROSAT*-HRI calibration report (David et al., 1997). It combines different components: the internal background, the externally-induced background from cosmic rays and the X-ray background (Galactic and extra-galactic). For our analysis we adopted the given standard values for the first two (pointing-independent) components. Terzan 5 is located near the Galactic plane, therefore the X-ray background, in particular the diffuse Galactic emission, is larger than average over the sky. Based on the results from Eger et al. (2010), we estimated this component as

---

[2] http://www.aips.nrao.edu/

[3] http://cxc.harvard.edu/ciao/

$3{\times}10^{-7}$ counts s^{-1} arcsec^{-2}. Compared to David et al. (1997), this is slightly above the standard value but still within the given range. The total expected HRI background level for this observation amounts then to 1.2×10^{-6} counts s^{-1} arcsec^{-2} in the 0.1 – 2.4 keV energy band.

Diffuse emission connected to Terzan 5 was searched for using concentric annular extraction regions 1′ thick centred on the GC, of internal radii 0 to 10′. We integrated the counts within each ring from the refilled HRI image and compared these to the afore-mentioned background component level. Figure 2 shows the surface brightness for the rings. All the extracted values agree within 1 σ and are compatible with the expected background. The innermost region, somewhat brighter than the others, is still within less than 2σ deviation from the expected background. The diffuse emission detected with *Chandra* (Eger et al., 2010) as well as un-removed point sources are likely to contribute to the flux measured in this innermost ring. In addition there might still be some contamination from the wings of the PSF of removed point-sources or a contribution from a transient source, a common phenomenon in dense GCs like Terzan 5 (see e.g. Heinke et al., 2002).

The archival HRI data confirm the previous results of Eger et al. (2010) and show no indication of emission above the Galactic diffuse component beyond 2′.5 away from Terzan 5. The extended X-ray emission connected to Terzan 5 seems therefore to be very localised, a result not accessible with the small-FoV *Chandra* data analysed in Eger et al. (2010).

3.2. INTEGRAL

The non-thermal X-ray emission detected by Eger et al. (2010) might be detectable in the hard X-ray regime by *INTEGRAL* if it extends to this energy band. For this source, of un-absorbed flux $5.5{\times}10^{-13}$ erg cm^{-2} s^{-1} and spectral index of about 0.9 in the 1 – 7 keV band (Eger et al., 2010), a flux of $4.9{\times}10^{-12}$ erg cm^{-2}s^{-1} in the 17 – 60 keV band is expected. This might be within the reach of *INTEGRAL*, which can detect sources down to $3.7{\times}10^{-12}$ erg cm^{-2} s^{-1} in the same band (Krivonos et al., 2010) near the Galactic centre (and also at the position of Terzan 5).

4. Other wavelengths

Infrared and ^{12}CO survey data were also studied, to gather information about the environment from dust and molecular gas content. A gradient in infrared emission in the direction perpendicular to the Galactic plane was found. For the whole region a very low average molecular gas column density was measured. No significant local features were found that could hint of peculiar conditions in the ISM close to the GC.

4.1. Far infrared data

The Infrared Astronomical Satellite (*IRAS*) archival data, here from the IRIS data reduction chain (Miville-Deschêne & Lagache, 2005), provides full-sky coverage at 4 wavelengths (12, 25, 60 and 100 μm). The angular resolution (4.2′ at 100 μm) is sufficient to distinguish differences on the scale of the regions considered here. Bright point-like sources from the *IRAS* catalogue (Beichman et al., 1988) were removed when estimating the average flux in the regions. After comparison to *Spitzer* maps[4], the limiting flux for source exclusion was set in the 12 μm band, where the contribution from stars is largest, to exclude at least the two *IRAS* point-like sources[5] closest to Terzan 5, corresponding to the GC itself and a nearby bright star.

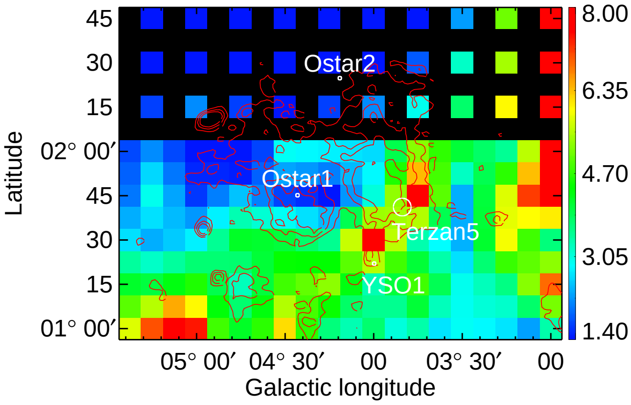

Fig. 3. Map of n_{H_2} derived from the ^{12}CO emission in the 3 to 10 km/s velocity range (roughly equivalent to a distance range of 1 to 3 kpc) overlaid with contours from the 11 cm data (for levels 0.07, 0.095 and 0.12 Jy/beam) and selected objects (see Section 5). The Terzan 5 circle indicates the half-mass radius of the GC. Colour scale normalised by 10^{20} cm^{-2}. The map was blanked where no value was available.

A flux density gradient is observed across the region, with a factor 2 decrease when moving away from the Galactic plane, with the lowest fluxes measured for region 12, the furthest away from the Galactic plane. Visual inspection of *IRAS* and *Spitzer* maps did not reveal any obvious extended structure in this region apart from Terzan 5 itself, where star crowding would mask any truly extended emission component.

4.2. Molecular gas and ^{12}CO data

The largest-coverage molecular-gas-tracer map of the Galactic plane was compiled by Dame et al. (2001), hereafter DA01, from the data of several surveys of the CO rotational transition 1 – 0 emission line. We extracted the temperature values against velocity from their publicly available[6] data cube. The values were integrated over the relevant velocity range, over the spatial extension of the region and finally converted into an hydrogen column density n_{H_2} (cm^{-2}) using the conversion factor $1.8{\times}10^{20}$ cm^{-2} K^{-1} km^{-1} s from DA01.

Using the close-case distance estimates from a Galactic rotation model (here following Clemens, 1985; Nakanishi & Yoshiabi, 2003), we selected the boundary velocities to bracket the distance to Terzan 5 (5.9 kpc): 20 km/s (≈5 kpc) and 120 km/s (≈7.3 kpc). The complete range provided by DA01 was also considered (from minus to plus 170 km/s). The estimated n_{H_2} are very low, as illustrated in Figure 3, compatible with zero in some regions, notably region 12 in all velocity ranges. The maximum values are measured in regions 6 and 9, with respectively 2.6 and $4.5{\times}10^{21}$ cm^{-2} in the full velocity range and 3.4 and $3.3{\times}10^{20}$ cm^{-2} in the velocity range compatible with the distance to Terzan 5. These values are comparable to other regions at similar Galactic latitude, where the latitude gradient of n_{H_2} was shown to be large (DA01). The neighbouring giant molecular cloud Bania Clump 2 mentioned in DA01 does not extend to this region. Most of the measured column density is associated to velocity range v <20 km/s (distances below 5 kpc). We interpret it as the cumulative emission from the diffuse molecular gas near the Galactic plane along the line of sight. Marginally significant structures found from visual inspection of the data cube are discussed in Section 5. The slightly larger values of n_{H_2} for regions 6 and 9 correspond to the shorter distance of these regions to the Galactic plane. Region 12 is the furthest away from the Galactic plane, away from distinct high-latitude features, so the null result (to the sensitivity of the available data) is not surprising.

---

[4] http://irsa.ipac.caltech.edu/applications/Cutouts/

[5] Catalogue accessed from Vizier (Ochsenbein et al., 2000).

[6] http://www.cfa.harvard.edu/mmw/obtainingData.html

5. Catalogue search

Previously identified objects potentially relevant to our study were searched with the help of the CDS online tools[7]. There appears to be no particularly energetic object in the region that could straightforwardly generate the entire observed radio emission. A few objects are worth mentioning (shown in Figure 4). The large radio source east of region 12 is SNR WR143. Two active galactic nuclei have been identified, one on each side of region 12, both as bright radio point sources. Two O type stars are found, one near the centre of region 10, the other north of Terzan 5. Both stars seem to be at a distance below 2 kpc (Reed, 2005). Figure 3 shows n_{H_2} for a compatible velocity range, with a local minimum coincident with one of the stars, labelled 'Ostar1' in the figure and catalogued as 2MASS J17491016-2414211. This may hint of a previous interaction between the star and molecular gas leading to a cavity. The data is too sparse near the other star to make any statement. Based on the *IRAS* source catalogue (Beichman et al., 1988) and young stellar object (YSO) selection criteria from *IRAS* colours (Junkes et al., 1992), two candidate YSOs were identified, one of them (labelled as 'YSO1') close to a radio hot spot and possibly a ^{12}CO one. All the other bright radio hot spots were previously catalogued (Reich et al., 1990a) but we found no additional published information on them.

6. Constraints on non-thermal emission processes

Based on the collected measurements, this Section focuses on testing non-thermal radiation processes that may generate the emission around Terzan 5. The energetics of the detected radio structures are constrained in Section 6.1. The particular properties of regions 10, 11 and 12 are discussed in Sections 6.2 to 6.4. Potential associations between Terzan 5 and region 11 or 12 are discussed. Section 6.5 examines the origin of the diffuse X-ray emission found by Eger et al. (2010).

While a physical connection between the structures seen around the direction of Terzan 5 (Figures 1 and 4) and the GC itself cannot be affirmed, it is assumed hereafter that they are all located at the same distance of 5.9 kpc. For the interpretation of the radio data, it is further assumed that synchrotron radiation (SR) emission is the dominant scenario. If the electron energy distribution follows a power law of index p, $N(E)dE = \kappa E^{-p} dE$, the radio spectral index α of the SR emission is $\alpha = (p-1)/2$. Typical values (Longair, 1992) for α are: for centre-filled supernova remnants (SNR) $\alpha \approx$ -0.3 – 0.0, for SNR shells $\alpha \lesssim -0.5$ and for the Galactic radio GHz range emission $\alpha \approx$ -0.9 – -0.8. In the absence of radio index measurements, we assume for all regions $\alpha = -0.8$. Along with this, a Bremsstrahlung scenario is investigated for region 10.

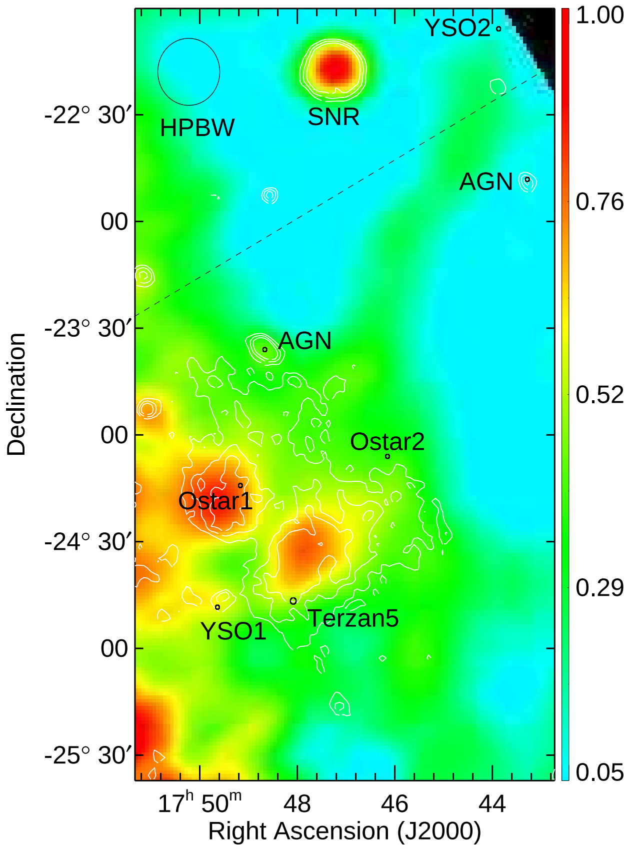

Fig. 4. Radio map from the Effelsberg Galactic plane surveys at 21 cm (in Jy/beam). Contours from the 11 cm map (for levels 0.07, 0.095 and 0.12 Jy/beam), selected catalog objects as well as the HPBW for the 21 cm data are over-plotted. The Terzan 5 circle indicates the half-mass radius of the GC. The dashed line indicate the radio scan direction at 21 cm.

6.1. Synchrotron radiation energetics

To estimate the energy in the radio structures assuming SR emission, the minimum energy condition (MEC) is used, as reviewed in Miley (1980). The MEC density of a radio source can be written as $u_{me} = (7/3)(B_{me}^2/8\pi)$ erg cm^{-3} and corresponds almost (but not exactly) to the equi-partition of energy between non-thermal particles and the magnetic field. For the frequency interval ν = 0.01 — 100 GHz and assuming a spectral index $\alpha = -0.8$, the corresponding magnetic field, in μG (for frequencies in GHz), is given by:

$$B_{me} = 140 \quad \left(\frac{\nu_0}{1\mathrm{GHz}}\right)^{0.22} \quad \left[\frac{S_0}{(1\mathrm{Jy})}\,\frac{(1\mathrm{arsec}^2\ 1\mathrm{kpc})}{\theta_x\,\theta_y\,s}\right]^{2/7} \qquad (2)$$

where θ_x and θ_y are the extent of the radio source on the plane of the sky in orthogonal directions, s is the path length through the source along the line of sight and ν_0 is the frequency where the flux S_0 is measured.

The MEC is assessed from the measurements of Table 2, for ν_0 = 2.7 GHz. It is assumed that region 1 is spherically symmetric with a radius of 15 pc and that regions 3 to 10 extend by the

---

[7] http://cdsweb.u-strasbg.fr/

	region												
	1	2	3	4	5	6	7	8	9	10	11	12	13
Wavelength [cm]	Average radio flux density (error) [kJy/sr]												
11	62.60	39.56	64.44	28.16	18.31	41.39	45.06	25.56	8.41	61.58	67.21	12.89	7.00
	(9.39)	(6.87)	(6.43)	(6.35)	(6.94)	(5.10)	(4.42)	(4.35)	(5.21)	(10.20)	(5.85)	(2.04)	(6.94)
21	60.88	63.76	74.05	33.94	40.69	81.75	55.71	35.54	50.63	86.67	73.53	18.54	1.29
	(17.74)	(12.73)	(11.84)	(11.93)	(12.91)	(9.47)	(8.00)	(8.23)	(9.66)	(18.97)	(10.67)	(4.07)	(4.30)

Table 2. Measurements extracted for the regions from the Effelsberg radio maps (Reich et al., 1990a,b). Regions 4, 5, 8 and 13 might indicate local background levels at 11 and 21 cm.

same 30 pc along the line of sight ($s = 30$ pc). The regions 10 to 12 are assumed to be structures where s equals the minimum extension of the source in the plane of the sky, estimated here for a distance of 5.9 kpc. Since the strength of B_{me} scales only with $(S_0/s)^{2/7}$, the uncertainties on the actual path lengths and the flux measurements are not critical to derive orders of magnitude. Under these assumptions, energetics for all the regions fall between a few 10^{48} ergs and more than 10^{49} ergs. The values for u_{me}, B_{me} as well as the total energy E_{me} (in particles and in the magnetic field) in each region are given in Table 3. These values serve as references in the following region-by-region discussions.

6.2. The O star and region 10

Region 10 is located north-east of Terzan 5. It does not overlap with the GC but contains an O star at a distance shorter than 2 kpc (see Section 5). Even though an association with the GC cannot be excluded, we now assume that region 10 is related to the O star, which could serve as source of ionising radiation for a Bremsstrahlung scenario. There are indications for a hole in the ^{12}CO distribution at distances between 1 and 3 kpc consistent with the location and potentially the distance of the O star. In the Bremsstrahlung picture the O star would ionise the embedding molecular material causing this hole in the ^{12}CO distribution. The ionised material would then emit Bremsstrahlung (e.g. Vasquez et al. , 2010). In such a scenario, n$_e$ would be comparable to the molecular gas density, of the order of 1 – 10 cm^{-3}. A flux density from region 10 of 14 $(T/10^4\,\mathrm{K})(n_e/10\,\mathrm{cm}^{-3})$ Jy would be expected, in broad agreement with the observed value. The expected Bremsstrahlung spectrum would be flat in the radio range ($\alpha \approx -0.1$). As visible in Figure 4, the features at 11 and 21 cm corresponding to region 10 do not match exactly. The possibility remains therefore that the set of properties used here for this region do not accurately describe it. Observation at higher spatial resolution may settle this issue.

6.3. Accumulation of relativistic electrons in region 11

The enhanced emission in region 11 covers the location of Terzan 5 and extends from there to the north-west of the GC, away from the Galactic Plane.

6.3.1. Evidence from the radio maps

The radio emission in region 11 represents in the MEC a total energy of 9.2×10^{48} ergs. For SR emission peaking at a few GHz in the MEC magnetic field of about 10 μG (see Table 3), electrons with an energy of about 10 GeV would be required (see e.g. Longair, 1992). Following Aharonian (2004), the cooling time of these electrons in such a magnetic field would be about 10^7 years. This scenario could be tested by the radio index, as radio spectral indices of -0.3 – 0.0 are typical of pulsar wind nebulae (PWNs, see Gaensler & Slane, 2006). Sampling the radio index within region 11 could then be used to estimate the electron production time scale, expected to be shorter than the cooling time if no spectral steepening was found.

6.3.2. Possible association with Terzan 5

Given the geometry of the radio feature covered by region 11, the large population of msPSRs in the GC could be the source of the radio-emitting electrons. Assuming that Terzan 5 contains 180 msPSRs (Abdo et al., 2010), each injecting energy on average at a moderate rate of 10^{33} ergs/s in electrons into the surroundings, about 2×10^6 years would be needed to build up the total electron population. This time scale is shorter than the cooling time estimated above, so this scenario seems viable.

The radio structure covered by region 11 extends from Terzan 5 in a direction roughly perpendicular to the Galactic plane. Based on the energy density given in Table 3 and assuming for the ISM a density of 0.1 cm^{-3} and a temperature of 10^5 K (see e.g. Aavage & de Boer, 1981), this radio structure would seem to be mildly over-pressured (by a factor of 3) with respect to the surrounding gas. It could therefore be expected to expand, preferentially in the direction of the Galactic density gradient, as observed. In this scenario, the expansion of the bubble is driven by the difference between the internal and external pressures (p_{int} and p_{ext}) over the surface S where they exert, with $F_p \sim (p_{int} - p_{ext}) \times S$. It is limited by the ram pressure of the surrounding medium, $F_{ram} \sim C\frac{1}{2}S\,v^2\rho_{ext}$ according to Churazov et al. (2001), with C the drag coefficient, v the expansion velocity and ρ_{ext} the density outside the bubble. The maximum terminal expansion velocity is then given by:

$$v \sim \sqrt{\frac{2}{C}\frac{p_{int} - p_{ext}}{\rho_{ext}}} \qquad (3)$$

For $C = 0.75$ (Churazov et al., 2001), $v \sim 80\,(n/0.1\mathrm{cm}^{-3})$ km/s. At this constant velocity, of the order of 10^6 years are needed to expand by 100 pc. These numbers are in rough agreement with the production timescale of the electron population in region 11.

Another mechanism operating at the location of Terzan 5 could potentially displace radio-emitting plasma produced in the GC in the direction perpendicular to the Galactic plane. Terzan 5 is placed in the onset region of the Galactic wind of our Galaxy, where the bulk motion flow of the wind material is expected to exceed 100 km/s (Everett et al., 2008). This Galactic wind could push away material originating in Terzan 5 even faster than the pressure imbalance discussed in the previous paragraph.

Detection of radio polarisation in this region, challenging at the distance of Terzan 5 (see e.g. the discussion on polarisation horizon in Landecker et al., 2010), would support a

	region											
	1	2	3	4	5	6	7	8	9	10	11	12
B_{me} [μG]	10.3	8.9	10.3	8.1	7.2	9.1	9.3	7.9	5.7	11.4	9.5	5.6
u_{me} [10^{-12} erg cm^{-3}]	9.8	7.4	9.8	6.1	4.8	7.7	8.0	5.8	3.0	12	8.4	2.9
E_{me} [10^{48} erg]	2.1	8.1	11	6.7	5.3	19	20	15	7.5	2.8	12	29

Table 3. Magnetic field strength, energy density and energetics for the regions computed according to the MEC. (see text for details).

plasma plume scenario. These dynamical models could be further tested against the proper motion of the GC. For instance, in 2×10^6 years and for a velocity in the plane of the sky of 50 km/s, a 100 pc long structure could be generated in the direction of motion. Conversely, too high a velocity or an incompatible direction of proper motion would exclude the proposed association between the radio feature in region 11 and Terzan 5.

6.4. The large-scale ridge in region 12

The ridge-like radio structure seen in region 12 stands out for its length and apparent alignment with Terzan 5. It is more visible in the 21 cm map (see Figure 4). Structures extending over similar linear scales and involving comparable energetics have been proposed (Fukui et al., 2009; Yamamoto et al., 2008) to result from highly collimated outbursts from either micro-quasars or stellar explosions. Such objects may be hosted by GCs like Terzan 5 but no equivalent central object or active region could be identified in relation to region 12. Higher sensitivity observations and dedicated investigations appear to be necessary to establish a full emission scenario for this region.

6.5. Revisiting the diffuse X-ray emission around Terzan 5

6.5.1. Non-thermal Bremsstrahlung

The molecular gas and infrared data can be used to test a non-thermal Bremsstrahlung origin for the extended diffuse X-ray emission in Terzan 5. In this scenario, electrons are deflected by target nuclei from the ambient medium. Therefore the intensity of the non-thermal X-ray emission should be correlated with the density of the local ISM. The absence of observational support from the ^{12}CO or infrared data for regions with high density of target material goes toward excluding a non-thermal Bremsstrahlung scenario for the diffuse X-ray emission in Terzan 5. More detailed investigation of the infrared data as well as higher resolution molecular gas tracer data may change this conclusion.

6.5.2. Inverse Compton scenario

One possible origin for the diffuse X-ray emission discovered by Eger et al. (2010) is X-ray IC radiation, usually accompanied by radio SR emission. The data gathered in this work can constrain this scenario.

The predicted radio SR emission is described by the frequency $\nu_{syn} = 120\,(\gamma/10^4)^2\,(B/1\mu\mathrm{G})\sin\phi$ MHz, with γ the Lorentz factor of the electrons, B the magnetic field and $\sin\phi$ the pitch angle of the electrons with respect to the magnetic field. For $\gamma \approx 30$, typical of IC radiation in the keV range (see Krockenberger & Grindlay, 1995), and neglecting $\sin\phi$, one gets $\nu_{syn} = 1.2\,(B/1\mu\mathrm{G})$ kHz. The SR flux relates to the IC flux by $F_{\mathrm{syn}}/F_{\mathrm{IC}} \approx (B^2/8\pi)/u_{rad}$, where $B^2/8\pi$ is the magnetic field energy density and u_{rad} is the radiation energy density responsible for the IC up-scattering. Assuming 1) that the X-ray flux of 5.5×10^{-13} erg cm^{-2} s^{-1} found by Eger et al. (2010) originates from IC emission, 2) that the MEC applies, giving a magnetic field $B = 10.3\,\mu$G, 3) that the radiation field is $u_{rad} = 40$ eV/cm^3 (Eger et al., 2010), a flux density of the order of 300 kJy at the related synchrotron frequency of about 12 kHz is expected. Extending a power-law spectrum up to the GHz range would require a spectral index around -1.0 for region 1.

The apparent validity of the IC emission hypothesis for the diffuse X-ray emission found by Eger et al. (2010) could be further tested with an accurate radio spectral index.

7. Conclusion

In this paper the surroundings of the GC Terzan 5 have been searched for indications of non-thermal diffuse emission. Several structures were isolated in the Effelsberg 21 and 11 cm surveys. The currently available data point towards a complex radio emitting region. However, interpretation of the radio structures is limited in the absence of reliable radio index. Future observations with high-frequency single-dish radio-telescopes or a dedicated re-analysis of the original Effelsberg data would improve this situation.

The most intriguing of these structures extends from the position of the GC to about 0.8° to the north-west. The energetics of this structure could be produced on a reasonable time scale by the population of msPSRs in Terzan 5 in a PWN scenario. Comparison of these time scales with the GC proper motion would provide a strong test to this model.

A smaller compact radio feature may be associated with an O star. Indication for a molecular gas cavity and order of magnitude agreement between the radio flux and a Bremsstrahlung model support this scenario. Confirmation of the molecular gas feature and of its distance are necessary tests to the proposed association.

There is an intriguing ridge-like extended radio source aligned with Terzan 5 roughly 1° north-east of the GC. In terms of energy content and spatial extent it shows similar characteristics to proposed remnants of highly asymmetric outbursts, either from a micro-quasar or the final explosion of a star. Since a GC may be the host of highly asymmetric explosions, such an origin cannot be excluded.

The presented multi-wavelength data is compatible with an IC origin for the recently discovered extended diffuse X-ray emission from the direction of Terzan 5. A non-thermal Bremsstrahlung scenario is not supported, although higher resolution data may change this conclusion.

Likewise, several negative results were obtained. No significant density of molecular material in the environment of Terzan 5 could be found, nor any clear hint of peculiar dust emission structure in the (low resolution) infrared data. The extension of the diffuse X-ray emission was limited to a $2'.5$ radius region around Terzan 5, to the sensitivity limit of the data.

Acknowledgements. The authors thank Karl-Heinz Mack (INAF, Istituto di Radioastronomia Bologna, Italy) for discussions about the radio analysis and Matthieu Renaud (CNRS, LPTA Montpellier, France) for sharing his expertise on *INTEGRAL*. This work was supported in part by the Polish Ministry of Science and Higher Education project N N203 380336.

References

Abdo, A.A. et al. (The Fermi LAT collaboration), 2009, Science, 325, 845A
Abdo, A.A. et al. (The Fermi LAT collaboration), 2010, A&A, 524, 75
Aharonian F.A. 2004, 'Very high energy cosmic gamma radiation : a crucial window on the extreme Universe', World Scientific Publishing
Baars, J.W.M. et al. 1977, A&A, 61, 99
Bednarek, W. & Sitarek, J. 2007, MNRAS, 377, 920
Beichman C. et al. 1988, 'IRAS Catalogs and Atlases Explanatory Supplement', NASA RP-1190, vol 1
Blackburn J.K. 1995, ASP Conf. Ser., vol. 77
Boese, F.G. 2000, A&AS, 141, 507B
Churazov, E. et al. 2001, ApJ, 554, 261
Clemens, D.P. 1985, ApJ, 295, 422C
Condon J.J. et al. 1998, AJ, 115, 1693
Dame, T.M., Hartmann, D. & Thaddeus, P., 2001, ApJ, 547, 792D
David L.P. et al., 1997, 'The ROSAT High Resolution Imager calibration report', Harvard-Smithsonian Center for Astrophysics, ftp://legacy.gsfc.nasa.gov/rosat/doc/hri/hri_report
Domainko, W. & Ruffert, M. 2005 A&A, 444, L33
Domainko, W. & Ruffert, M. 2008, AdSpR, 41, 518
Draine, B.T. & Li, A. 2007, ApJ, 657, 810D
Eger, P., Domainko, W. & Clapson, A.-C. 2010, A&A, 513, 66
Everett, J.E. et al. 2008, ApJ, 674, 258
Fender, R.P., Garrington, S.T., McKay, D.J. et al. 1999, MNRAS, 304, 865
Ferraro, F.R., Beccari, G., Dalessandro, E., et al. 2009, Nature, 462, 1028
Fruchter A.S. & Goss W.M. 2000, ApJ, 536, 865
Fukui, Y., Furukawa, N., Dame, T.M. et al. 2009, PASJ, 61, L23
Gaensler, B.M. & Slane, P.O. 2006, ARA&A, 44, 17
Green, D.A. 2009, BASI, 37, 45
Grindlay, J., Portegies Z.S. & McMillan, S. 2006, Nature Physics, 2, 116
Harris, W. E. 1996, AJ, 112, 1487
Heinke, C.O. et al. 2002, Bulletin of the American Astronomical Society, Vol. 34, p.1313
Heinke, C.O. et al. 2006, ApJ, 651, 1098
Isobe, N. et al. 2002, ApJ, 580, L111
Ivanova, N., Heinke, C.O., Rasio, F.A., Belczynski, K. & Fregeau, J. M. 2008, MNRAS, 386, 553
Johnston H.M., Verbunt, F. & Hasinger, G. 1995, A& A, 298, L21
Karovska M. et al. 2001, ASP Conference Proceedings, Vol. 238, 435
Klein, U., Mack, K.-H., Gregorini, L. & Vigotti, M. 2003, A&A, 406, 579
Kong, A.K.H., Hui, C.Y. & Cheng, K.S. 2010, ApJ, 712, 36
Koyama, K., Petre, R., Gotthelf, E.V., et al. 1995, Nature, 378, 255
Gopal-Krishna & Steppe, H. 1980, A&A, 88, 354
Krivonos, R. et al. 2010, A&A, 519, 107
Krockenberger, M. & Grindlay, J.E., 1995, ApJ, 451, 200K
Landecker, T.L. et al. 2010, A&A, 520, 80
Lanzoni B. et al. 2010, ApJ, 717, 653
Lesch, H. & Reich, W. 1992, A&A, 264, 493
Longair, M.S., 1992, 'High energy astrophysics. Vol.1: Particles, photons and their detection', Cambridge University Press
Miley, G. 1980, ARA&A, 18, 165
Miville-Deschłnes M.-A. & Lagache G. 2005, ApJSS, 157, 302
Nakanishi, H. & Yoshiaki S. 2003, PASJ, 55, 191N
O'Dea, C.P. et al. 2009, A&A, 494, 471
Ochsenbein F., Bauer P. & Marcout J. 2000, A&AS 143, 221
Okada, Y., Kokubun, M., Yuasa, T. & Makishima, K. 2007, PASJ, 59, 727
Paladini, R., Burigana, C., Davies, R.D. et al., 2003, A&A, 397, 213
Perner, R., Raymons, J. & Loeb, A., 2000, ApJ, 533, 658
Pooley, D. & Hut, P. 2006, ApJ, 646, L143
Ransom, S.M. 2008, in IAU Symposium, Vol. 246, IAU Symposium, ed. E. Vesperini, M. Giersz, & A. Sills, 291300
Reed B.C. 2005, AJ, 130,1652
Reich, W. et al. 1988, A&A, 191, 303
Reich, W., Reich, P. & Fürst, E. 1990, A&AS, 83, 539R
Reich, W., Fürst, E., Reich, P. & Reif, K. 1990, A&AS, 85, 633
Rybicki, G.B. & Lightman, A.P. 1979, 'Radiative processes in astrophysics', New York, Wiley-Interscience
Savage, B.D. & de Boer, K.S. 1981, ApJ, 243, 460S
Shara, M.M. & Hurley, J.R. 2002, ApJ, 571, 716
Junkes, N., Fuerst, E. & Reich, W. 1992, A&A, 261, 289
Vasquez, J., Cappa, C.E., Pineault, S. & Duronea, N.U. 2010, MNRAS, 405, 1976
Venter, C. & de Jager, O.C. 2008, AIPC, 1085, 277
Venter, C., de Jager, O.C. & Clapson, A.-C. 2009, ApJ, 696, L52
Yamamoto, H., Ito, S., Ishigami, S., et al. 2008, PASJ, 60, 715